

Precise Point Positioning Method for a Static Survey in a High Multipath Environment

Joseph M. Strus and James W. Sinko, *SRI International*

BIOGRAPHY

Joseph M. Strus is a Systems Analyst at SRI International where he has worked on precision navigation applications since 2001. Previously, he was a GPS Systems Engineer with the Government Systems Division of Rockwell Collins. Dr. Strus received his B.S. (1986) and Ph.D. (1994) in Mathematics from the University of Illinois at Urbana-Champaign.

James W. Sinko is a Principal Engineer at SRI International. He received his B.S. (Engineering Science) and M.S.E.E. from Stanford University, and his Ph.D. (EE) from the University of Rochester. Dr. Sinko has been with SRI since 1967, working with radar and aircraft systems. For the last nine years, he has been working with precision GPS for military and civil applications.

ABSTRACT

Precise point positioning (PPP) methods are generally considered to be point solution methods using undifferenced code and carrier phase measurements. Since the measurements are undifferenced, a means of reducing systematic errors in the measurements is generally used. Precise orbit and satellite clock values from IGS or other organizations are most often used to reduce system biases. PPP methods promise decimeter level positioning or better in stand-alone operation.

Many PPP methods rely on code phase. These methods are subject to code multipath and hence typically use long smoothing filters and L1/L2 measurements to reduce multipath. As a result, these methods take a long time to converge to decimeter level accuracies. However, once they do converge, they provide the means for kinematic applications. Other PPP methods are carrier phase only methods. Some of these methods are attempting various types of ambiguity resolution. These show some promise and are providing interesting results.

At SRI International, we often have need to provide a stationary survey in an environment that may have very high multipath. We are interested in rapidity of

convergence of stand-alone carrier phase positioning methods. We use an IGS rapid ephemeris. This paper describes a carrier phase only solution based on a method derived from weighted batch least squares. Preliminary results show reliable sub-decimeter positioning after six hours. We attempt to quantify the error behavior as the settling time is decreased. Results are compared with several alternative precise positioning methods. Also discussed are the numerical stability issues associated with methods of this type. The phase only method we derive is compared with several carrier smoothed code methods. The data used are from SPS receivers as well as from a PPS receiver.

INTRODUCTION

Precise point positioning (PPP) methods are generally considered to be point solution methods using undifferenced code and carrier phase measurements. Since the measurements are undifferenced, a means of reducing systematic errors in the measurements is used. This is generally accomplished by using one of several services which provide precise ephemerides and clocks, examples of which are the International GPS Service (IGS), or one of its associated processing centers, the National Geodetic Agency (formerly National Imagery and Mapping Agency), or National Resources of Canada [Kouba and Heroux, 2000; Kouba, 2000; Skone et al., 1996]. Thus, while the user *does not* need to supply a reference receiver, the user is effectively using a large number of reference stations. The user must also have some means of obtaining the ephemeris data, either via the Internet; or in the case of the commercial services such as Starfire, real-time corrections can be obtained via INMARSAT satellites.

We have used PPP for quickly (hours) establishing the location of reference stations for a rapidly deployed wide-area DGPS network. To hasten deployment, these reference stations are sometimes located in environments that have high amounts of code multipath. In normal operation, the reference stations reduce this multipath with a combination of long-term carrier smoothing and multipath maps. However, over shorter time periods, code

multipath is more difficult to reduce and this affects short-term survey accuracy. As a result, at sites with high multipath, it appeared justifiable to delete code measurements from the positioning process. We continue to use code measurements for outlier detection. The idea of exclusively relying on carrier phase for positioning has been used previously in GPS (Malys and Ortiz, 1989) and is similar to Doppler navigation. The elimination of code multipath comes at the expense of having to take measurements for a longer period of time—until there is significant movement of the satellite vehicles (SVs) across the sky.

Where we differ with previous attempts, we believe, is in the solution method. Previous authors have used recursive filters to sequentially process measurements. Here, we use only the simpler batch least squares method. The main reason for this is the simple derivation of the position covariance. This is important because we wanted to consider several different methods of processing the carrier phases over multiple epochs. These methods are (1) using undifferenced measurements, (2) single differences with a pivot satellite, (3) epoch to epoch differences, and (4) double differences. The techniques and their expected position variance are derived below. For some of the methods, this requires a matrix of size 50×50 or more to be inverted, but this is not a problem for even the most modest of current computers, even for real-time use. The derivations are for stationary applications, but they can be extended to dynamic cases (see Bisnath and Langley, 2002). Throughout, we assume a dual-frequency user and access to IGS ephemerides and clocks.

The IGS orbits and clocks are available as the ultra-rapid (the predicted part which is available for real-time applications is accurate to about a meter), rapid (better than a dm and available in 17 hours), and the final (accurate to 5 cm and available in two weeks). An important aspect of PPP is that it gives us a window into the performance of future global navigation system performance. The IGS rapid and final products are much more accurate than the broadcast parameters. This is due to a larger reference network, more inclusive modeling, and the ability to post process. However, even over the first few hours of the prediction interval, the IGS ultra-rapid orbit and clock predictions are much better than the broadcast orbits and clocks. This is largely due to lower data latency. When future Global Navigation Satellite Systems use almost continuous updates for the satellite orbit and clock data, they will be able to duplicate the IGS clock and orbit accuracies, even if there are no further improvements in SV clocks.

The paper is organized as follows. First we derive our carrier phase only basic linearized measurement equation. We then look at four different variations of this model and derive the position covariance for each method. In the

second part of the paper, we continue only with the method with the least expected position error. We use measurements collected from Continuously Operating Reference Station (CORS) sites and then from data collected at the SRI campus to validate the carrier phase only method. We show typical performance to be sub-decimeter using an IGS rapid orbit after six hours.

PROBLEM FORMULATION

A dual frequency GPS receiver makes code and carrier phase measurements on the frequencies L_i , $i=1,2$. A simplified code and carrier phase measurement model will now be described. The code pseudo-range measurement $P_i^j(t)$ and the carrier phase measurement $\Phi_i^j(t)$ for the j -th satellite on the i -th frequency at time t can be described by the following equations:

$$\begin{aligned} P_i^j(t) &= \rho^j(t) + c\delta^j(t) - c\delta(t) + \delta_{trop}(t) + \delta_{iono/L_i}(t) \\ &\quad + M^j(t) + E_i^j(t) \\ \Phi_i^j(t) &= \rho^j(t) + c\delta^j(t) - c\delta(t) + \delta_{trop}(t) - \delta_{iono/L_i}(t) \\ &\quad + m^j(t) + f_i^j(t) + \varepsilon_i^j(t) \end{aligned} \quad (1)$$

where ρ^j is the true range between satellite j and the user, c is the speed of light, δ^j is the j -th satellite clock error, δ is the receiver clock error, δ_{trop}^j is the tropospheric delay along the line of sight to the j -th satellite, δ_{iono/L_i}^j is the ionospheric delay at L_i and $f_i^j(t)$ is the float ambiguity of the j -th satellite at frequency i , M^j is code multipath and m^j is carrier phase multipath, and E_i^j is code measurement error and ε_i^j is carrier phase error (see Abdel-Salam et al., 2002).

The iono-free combination (IF) is formed to eliminate the dispersive effects on the code and carrier measurements. This combination can be written as

$$\begin{aligned} P_{IF}^j(t) &= \frac{L_1^2 * P_1^j(t) - L_2^2 * P_2^j(t)}{L_1^2 - L_2^2} \\ \Phi_{IF}^j(t) &= \frac{L_1^2 * \Phi_1^j(t) - L_2^2 * \Phi_2^j(t)}{L_1^2 - L_2^2} \end{aligned}$$

where L_1 and L_2 are the L1 and L2 frequencies, respectively.

Thus, (1) can be written at iono-free as

$$\begin{aligned}
P_{IF}^j(t) &= \rho^j(t) + c\delta^j(t) - c\delta(t) + \delta_{trop} + M_{IF}^j(t) + E_{IF}^j(t) \\
\Phi_{IF}^j(t) &= \rho^j(t) + c\delta^j(t) - c\delta(t) + \delta_{trop} \\
&\quad + m_{IF}^j(t) + f_{IF}^j(t) + \varepsilon_{IF}^j(t)
\end{aligned} \quad (2)$$

At this point several things should be noted about the equations in (2). The IF float ambiguities in (2) are floating point numbers and no attempt is made to exploit integer values on L1 or L2. The multipath and noise of the IF combination is approximately three times larger than the L1 or L2 measurements (Misra and Enge, 2001). For the remainder, we assume that the IF code multipath terms are so large and poorly behaved that the code measurements are unavailable.

To transform the measurements in (2) into the solution domain, first write

$$\rho^j(t) = \sqrt{(X^j(t) - X)^2 + (Y^j(t) - Y)^2 + (Z^j(t) - Z)^2} \quad (3)$$

where $\langle X^j(t), Y^j(t), Z^j(t) \rangle^T$ and $\langle X, Y, Z \rangle^T$ are the positions of the j -th satellite and the receiver, respectively. Linearizing (3) about the approximate position $\langle X_0, Y_0, Z_0 \rangle^T$ and writing $X = X_0 + dx$, $Y = Y_0 + dy$, $Z = Z_0 + dz$, the linearized observation equations can be written as

$$\begin{aligned}
\Phi_{IF}^j(t) &= \rho_0^j(t) - \left[\frac{X^j(t) - X_0}{\rho_0^j} \right] \Delta X - \left[\frac{Y^j(t) - Y_0}{\rho_0^j} \right] \Delta Y \\
&\quad - \left[\frac{Z^j(t) - Z_0}{\rho_0^j} \right] \Delta Z + c\delta^j(t) - c\delta(t) + \delta_{trop} \\
&\quad + m_{IF}^j(t) + f_{IF}^j(t) + \varepsilon_{IF}^j(t) .
\end{aligned}$$

From the basic linearized measurement model in (3), we now consider four different types of solution: (1) the time of arrival (TOA) model, (2) the time difference of arrival (TDOA) model, (3) epoch difference of arrival (EDOA) model, and (4) double difference (DD) model. Each of these has a different set of variables and a different geometry matrix. The following sections discuss these individually. In each section, we describe the variables and the matrix equations for the single epoch solution followed by the solution for the multiple epoch solution. After this, the results for the covariance of the position states is derived for each of the four methods based on a set of sample data as if the solution were obtained from a basic batch least squares method.

TOA Formulation

Single Epoch TOA

The states in the single epoch solution of the basic model (TOA) are station position coordinates, receiver, clock, and the float ambiguities for the satellites in view. Assuming M satellites are visible at time t , and using (3),

$$\begin{pmatrix} \Delta \rho^1 \\ \vdots \\ \Delta \rho^M \end{pmatrix} = \begin{bmatrix} x^1(t) & y^1(t) & z^1(t) & 1 & 1 & 0 & 0 \\ x^2(t) & y^2(t) & z^2(t) & 1 & 0 & 1 & \\ \vdots & \vdots & \vdots & & & & \ddots \\ x^M(t) & y^M(t) & z^M(t) & 1 & 0 & & 1 \end{bmatrix} \begin{bmatrix} \Delta X \\ \Delta Y \\ \Delta Z \\ -c\delta(t) \\ f_{IF}^1(t) \\ \vdots \\ f_{IF}^M(t) \end{bmatrix} \quad (4)$$

$$\text{where } x^j(t) = \frac{X^j(t) - X_0}{\rho_0^j}, \quad y^j(t) = \frac{Y^j(t) - Y_0}{\rho_0^j},$$

$$z^j(t) = \frac{Z^j(t) - Z_0}{\rho_0^j}, \text{ and}$$

$\Delta \rho^j = \Phi_{IF}^j(t) - \rho_0^j(t) - c\hat{\delta}^j(t) - \hat{\delta}_{trop}^j$ and the cap terms are estimates of the quantities in question. This is the basic block matrix for a single epoch of observation. Note that this matrix is not invertible.

Multiple Epoch TOA

In the single epoch case presented above, the receiver clock terms are indistinguishable from the float ambiguities and the resulting solution matrix is not invertible. Therefore, in the multiple epoch case, the initial clock term is not estimated (in effect single differenced out) and all following receiver clock estimates are relative to the first epoch.

Also, due to satellites rising and setting and cycle slips during the observation interval, the number of float ambiguities is variable and must be determined as the batch matrix is being built. In general then, assume that we have N time epochs and a total of S arcs where the float ambiguities are constant over an arc. Assume also there are $v(n)$ usable satellites visible at the n -th epoch.

Define $P = \sum_{n=1}^N v(n)$. Thus, P is the total number of observations. Then the design or geometry matrix G is $P \times (3+N-1+S)$.

So that building up the matrix in (4) over time, the matrix G looks like

$$G = \begin{bmatrix} x^1(t_1) & y^1(t_1) & z^1(t_1) & 1 & 0 & 1 & 0 \\ \vdots & \vdots & \vdots & \vdots & 0 & \vdots & \vdots \\ x^{v(1)}(t_1) & y^{v(1)}(t_1) & z^{v(1)}(t_1) & 1 & 0 & 0 & 1 \\ x^1(t_2) & x^1(t_2) & x^1(t_2) & 1 & 1 & 0 & 0 \\ \vdots & \vdots & \vdots & 0 & \vdots & 0 & \vdots \\ x^{v(2)}(t_2) & y^{v(2)}(t_2) & z^{v(2)}(t_2) & 1 & 0 & 0 & 1 \\ \vdots & \vdots & \vdots & \vdots & \vdots & \vdots & \vdots \\ x^1(t_N) & y^1(t_N) & z^1(t_N) & 0 & 1 & 1 & 0 \\ \vdots & \vdots & \vdots & 0 & \vdots & \vdots & \vdots \\ x^{v(N)}(t_N) & y^{v(N)}(t_N) & z^{v(N)}(t_N) & 1 & 0 & 0 & 1 \end{bmatrix} \quad (5)$$

where for simplicity we have assumed the same satellites are in view for the first N epochs. Figure 1 shows the growth of the number of states and the number of measurements in the batch least squares solution as a function of time for day 110 year 2003. Probabilistic methods for the matrix size can also be derived (see Zumberge et al., 1997). Generally, though, it is impossible to quantify the size of this matrix in advance because the receiver cycle slips and other losses of lock cannot be quantified in advance.

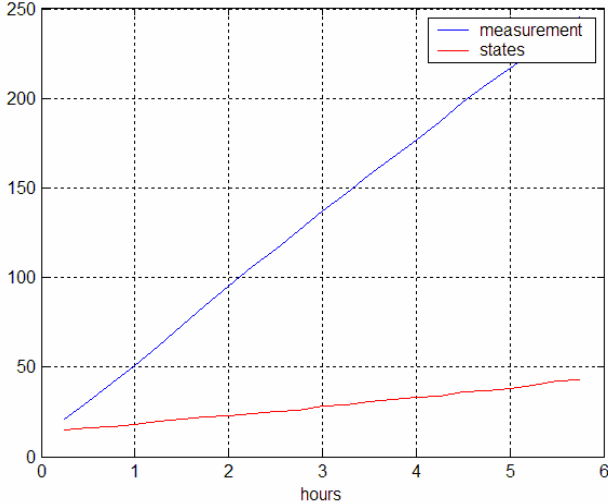


Figure 1. Number of states and measurements in batch least squares solution

TDOA Formulation

Single Epoch Solution

This section describes the problem from the standpoint of eliminating the receiver clock bias at each epoch. This is done by using a common satellite (pivot) for each epoch and differencing the measurements from the common satellite. For single epoch code positioning, this is usually referred to as TDOA. The TDOA method removes the receiver clock value at the expense of adding noise to the

measurements. However, it is more or less well known that for standard GPS point positioning (single epoch, code solution), that the position error variance for single difference (TOA) is the same as for non-differenced (TDOA) (Shin et al., 2000).

Returning to the measurement equation in (3), and performing the first difference, for the j -th and k -th satellites at the same time,

$$\begin{aligned} \Delta\Phi_{IF}^{jk}(t) &= \rho^j(t) - \rho^k(t) + c\delta^j(t) - c\delta^k(t) + \delta_{trop}^j - \delta_{trop}^k \\ &\quad + m_{IF}^j(t) - m_{IF}^k(t) + f_{IF}^j(t) - f_{IF}^k(t) + \varepsilon_{IF}^j(t) \\ &= \Delta\rho^{jk}(t) - c\Delta\delta^{jk}(t) + \Delta\delta_{trop}^{jk} + f_{IF}^{jk}(t) + \varepsilon \end{aligned}$$

and hence the linear matrix equation becomes

$$\begin{pmatrix} \Delta\Delta\rho^{1M} \\ \vdots \\ \Delta\Delta\rho^{(M-1)M} \end{pmatrix} = \begin{bmatrix} \Delta x^{1M}(t) & \Delta y^{1M}(t) & \Delta z^{1M}(t) & 1 & 0 \\ \vdots & \vdots & \vdots & \vdots & \vdots \\ \Delta x^{(M-1)M}(t) & \Delta y^{(M-1)M}(t) & \Delta z^{(M-1)M}(t) & 0 & 1 \end{bmatrix} \times \begin{bmatrix} \Delta X \\ \Delta Y \\ \Delta Z \\ f_{IF}^{1M}(t) \\ \vdots \\ f_{IF}^{(M-1)M}(t) \end{bmatrix} \quad (6)$$

where $\Delta\Delta\rho^{jk} = \Delta\rho^j - \Delta\rho^k$ and $\Delta x^{jk}(t) = x^j(t) - x^k(t)$.

Multiple Epoch TDOA

When multiple epochs are used, the receiver clock terms for each epoch are canceled. This leaves us with an invertible solution and the clock terms are not estimated.

Unfortunately, every time the pivot satellite needs to change, a new ambiguity must be estimated. This implies that to maximize the number of epochs that use a particular ambiguity, we would use a satellite that is in track for a long time. Assume that we have N time epochs and a total of S single difference arcs where the single difference float ambiguities are constant over an arc.

Assume also there are $v(n)$ usable satellites visible at the n -th epoch. Define $P = \sum_{n=1}^N v(n)$. Thus $(P-N)$ is the total number of observations. Then the G matrix to be considered is $(P-N) \times (3+S)$.

Building up the matrix in (6) over time, the matrix G looks like

$$G = \begin{bmatrix} \Delta x^{1v(1)}(t_1) & \Delta y^{1v(1)}(t_1) & \Delta z^{1v(1)}(t_1) & 1 & 0 & 0 & 0 \\ & \vdots & & 0 & \ddots & 0 & \ddots \\ \Delta x^{(v(1)-1)v(1)}(t_1) & \Delta y^{(v(1)-1)v(1)}(t_1) & \Delta z^{(v(1)-1)v(1)}(t_1) & 0 & 1 & 0 & 0 \\ \Delta x^{1v(2)}(t_2) & \Delta y^{1v(2)}(t_2) & \Delta z^{1v(2)}(t_2) & 1 & 0 & 0 & 0 \\ & \vdots & & 0 & \ddots & 0 & \vdots & \ddots \\ \Delta x^{(v(2)-1)v(2)}(t_2) & \Delta y^{(v(2)-1)v(2)}(t_2) & \Delta z^{(v(2)-1)v(2)}(t_2) & 0 & 1 & 0 & 0 \\ & \vdots & & & \vdots & & \vdots \\ \Delta x^{1v(n)}(t_N) & \Delta y^{1v(n)}(t_N) & \Delta z^{1v(n)}(t_N) & & & 1 & 0 \\ & \vdots & & 0 & & \ddots & \\ \Delta x^{(v(n)-1)v(n)}(t_N) & \Delta y^{(v(n)-1)v(n)}(t_N) & \Delta z^{(v(n)-1)v(n)}(t_N) & & & 0 & 1 \end{bmatrix} \quad (7)$$

where for simplicity we have assumed that at the N -th epoch the single difference ambiguities in use are $S - v(N) + 1, \dots, S$. In practice, the size of this matrix is similar to that shown in Figure 1. Note that the TDOA PDOP (position dilution of precision) and TOA PDOP are not equal as is true for the code only case.

EDOA Formulation

Single Epoch Solution

This section returns to the TOA method described in the first section, and takes differences over successive epochs; the differences are taken with respect to a fixed satellite over time. We call this Epoch Difference of Arrival (EDOA). This method reintroduces the receiver clock errors (actually the differences in receiver clock errors) over an epoch. However, the float ambiguities are eliminated.

The measurement equation in this case has the form

$$\begin{aligned} \nabla \Phi_{IF}^{1,0}(t_1) &= \rho^j(t_1) - \rho^j(t_0) + c\delta^j(t_1) - c\delta^j(t_0) + \delta_{trop}^j(t_1) \\ &\quad - \delta_{trop}^j(t_0) + m_{IF}^j(t_1) - m_{IF}^j(t_0) + \varepsilon_{IF}^j(t) \\ &= \nabla \rho^{jk}(t) - c\nabla \delta^{jk}(t) + \nabla \delta_{trop}^{jk} + \varepsilon \end{aligned}$$

and linearizing gives

$$\begin{pmatrix} \nabla \Delta \rho^1 \\ \vdots \\ \nabla \Delta \rho^M \end{pmatrix} = \begin{bmatrix} \nabla x^1(t_1) & \nabla y^1(t_1) & \nabla z^1(t_1) & 1 \\ \vdots & \vdots & & \\ \nabla x^M(t_1) & \nabla y^M(t_1) & \nabla z^M(t_1) & 1 \end{bmatrix} \begin{bmatrix} \Delta X \\ \Delta Y \\ \Delta Z \\ -c\nabla \delta(t) \end{bmatrix} \quad (8)$$

where $\nabla \Delta \rho^j = \Delta \rho^j(t_1) - \Delta \rho^j(t_0)$ and $\nabla x^j(t_1) = x^j(t_1) - x^j(t_0)$.

Multiple Epoch EDOA

In this case the extension to multiple epochs presents no particular problems other than that a clock state is added for each epoch.

With N time epochs assume there are $v(n)$ satellites visible and in continuous track from the $(n-1)$ -st to n -th epoch. Define $P = \sum_{n=2}^N v(n)$. The G matrix in this case is then $P \times (3+N-1)$.

So that building up the matrix in (8) over time, for the first set, the matrix G looks like

$$G = \begin{bmatrix} \nabla x^1(t_2) & \nabla y^1(t_2) & \nabla z^1(t_2) & 1 & & & \\ & & & \vdots & & & 0 \\ \nabla x^{v(1)}(t_2) & \nabla y^{v(1)}(t_2) & \nabla z^{v(1)}(t_2) & 1 & & & \\ \nabla x^1(t_3) & \nabla x^1(t_3) & \nabla x^1(t_3) & 0 & 1 & & \\ & \vdots & & 0 & \vdots & & 0 \\ \nabla x^{v(2)}(t_3) & \nabla y^{v(2)}(t_3) & \nabla z^{v(2)}(t_3) & 1 & & & \\ & \vdots & & & & & \\ \nabla x^1(t_N) & \nabla y^1(t_N) & \nabla z^1(t_N) & & & & 1 \\ & \vdots & & & & & \vdots \\ \nabla x^{v(N)}(t_N) & \nabla y^{v(N)}(t_N) & \nabla z^{v(N)}(t_N) & & & & 0 \\ & & & & & & \vdots \\ & & & & & & 1 \end{bmatrix} \quad (9)$$

In practice, the size of this matrix is similar to that shown in Figure 1.

DD Formulation

Single Epoch Solution

The states in the double difference formulation are simply the station coordinates. The observation model is obtained by differencing both over time and over a pivot satellite. This method has been used in the past in the Geodetic Absolute Positioning (GASP) program developed at the Defense Mapping Agency (Malys and Ortiz, 1989).

The linearized measurement model in this case has the form

$$\begin{pmatrix} \nabla\Delta\Delta\rho^{1M} \\ \vdots \\ \nabla\Delta\Delta\rho^{(M-1)M} \end{pmatrix} = \begin{bmatrix} \nabla\Delta x^{(1)M}(t_1) & \nabla\Delta y^{(1)M}(t_1) & \nabla\Delta z^{(1)M}(t_1) \\ \vdots & \vdots & \vdots \\ \nabla\Delta x^{(M-1)M}(t_1) & \nabla\Delta y^{(M-1)M}(t_1) & \nabla\Delta z^{(M-1)M}(t_1) \end{bmatrix} \begin{bmatrix} \Delta X \\ \Delta Y \\ \Delta Z \end{bmatrix} \quad (10)$$

where $\nabla\Delta\Delta\rho^{jk} = \Delta\rho^{jk}(t_1) - \Delta\rho^{jk}(t_0)$ and $\nabla\Delta\Delta x^{jk} = \Delta x^{jk}(t_1) - \Delta x^{jk}(t_0)$.

Multiple Epoch DD

In this case the extension to multiple epochs presents no particular problems. Assuming N time epochs, define $v(n)$ as the number of satellites visible and in continuous track

from the $(n-1)$ -st to n -th epoch. Define $P = \sum_{i=2}^N v(n)$. Thus,

P is the total number of observations. Then the G matrix to be considered is $P \times 3$.

Building up the matrix in (10) over time, for the first set, the matrix G looks like

$$G = \begin{bmatrix} \nabla\Delta x^{1v(1)}(t_2) & \nabla\Delta y^{1v(1)}(t_2) & \nabla\Delta z^{1v(1)}(t_2) \\ \vdots & \vdots & \vdots \\ \nabla\Delta x^{(v(1)-1)v(1)}(t_2) & \nabla\Delta y^{(v(1)-1)v(1)}(t_2) & \nabla\Delta z^{(v(1)-1)v(1)}(t_2) \\ \vdots & \vdots & \vdots \\ \nabla\Delta x^{1v(1)}(t_N) & \nabla\Delta y^{1v(1)}(t_N) & \nabla\Delta z^{1v(1)}(t_N) \\ \vdots & \vdots & \vdots \\ \nabla\Delta x^{(v(N)-1)v(N)}(t_N) & \nabla\Delta y^{(v(N)-1)v(N)}(t_N) & \nabla\Delta z^{(v(N)-1)v(N)}(t_N) \end{bmatrix} \quad (11)$$

Covariance Analysis

To evaluate the position variance for the four methods described above, sample satellite data are taken from week 1215 day 0. Earth position of the user is taken as the equator. Observations are at 15 minutes. In general, all the position solution methods can be written as $\rho = Gx$, where ρ are the measurements and x are the variables to be estimated. The batch least squares solution is then obtained as $x = (G^T G)^{-1} G^T \rho$ and the covariance of x can be written as $\text{cov } x = \sigma^2 (G^T G)^{-1}$ where σ^2 is the assumed equal variance of the measurements ρ and G are any of the matrices in equations 5, 7, 9, and 11.

For the analysis presented above, PDOP is defined as $PDOP = \sqrt{\text{var}(X) + \text{var}(Y) + \text{var}(Z)}$ where X, Y, Z are the position variables and $\text{var}(\cdot)$ is the variance. To scale the various measurements so that all four methods are comparable, the TDOA and EDOA PDOPs must be multiplied by $\sqrt{2}$ and the DD PDOP must be multiplied

by 2. Figure 2 shows the PDOP of the resulting position estimate for the four methods.

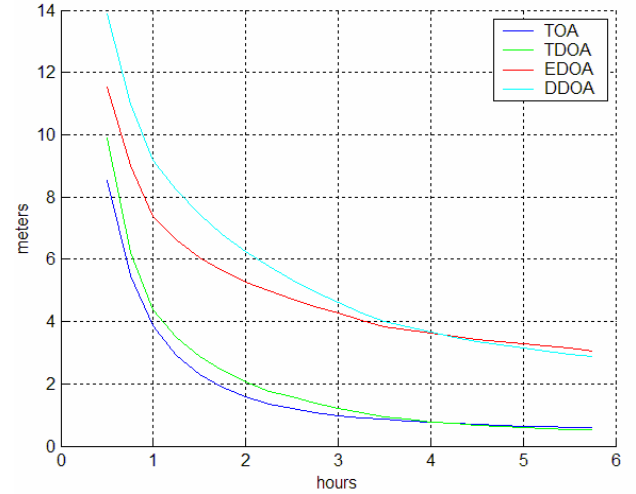


Figure 2. Expected 1σ 3-D error from four solution methods

The results are more or less consistent with the observation that TOA PDOP should be close to TDOA PDOP and EDOA PDOP should be close to DDOA PDOP.

Measurement Models

This section looks at error mitigation in the measurements used in PPP. Since no differential receiver is available to cancel system errors, accurate attention must be given to the error models in PPP. The compensations we apply are for solid earth tides, relativity, earth rotation, and the satellite antenna offset. For the troposphere, we assume that we have a nearby weather station to estimate the zenith tropo delay using the Sasstamoinan model and then the dry and wet zenith tropospheric delay are estimated using the Niell mapping function (Niell, 1996). We do not model other effects such as ocean loading and antenna phase windup. Furthermore, at this point, we weight the measurements equally.

We have not been pleased with the results we have obtained using interpolated clock data, so we have restricted our processing to 15-minute epochs to match the availability of IGS clock and ephemeris data.

RESULTS

CORS Data

The first test of the algorithms was done on data from the National Geodetic Survey's CORS network. We chose data from the United States Naval Observatory (USNO). The data at this site are taken from an Ashtech timing

receiver driven by one of the hydrogen maser references at the USNO. The carrier phase data are therefore of exceptional quality featuring low multipath and small carrier phase noise. The date of the data collection is day 110 of 2003. Six hours of data were decimated to 900 seconds and an elevation mask angle of 10 degrees was used. The IGS precise orbit and clock were used.

Figure 3 shows the result of the processing. The results are compatible with that predicted from the covariance analysis in the short term (1–2 hours) but not as good in the long term. In the first hour the accuracy is limited by the noise and multipath in the IF phase measurement (about 2 cm). The random errors are multiplied by the PDOP to give an expected error of 60 cm after 15 minutes, 15 cm after 30 minutes, and 8 cm after 1 hour. This is consistent with what was observed. The errors level off after a few hours. This is most likely due to unmodeled measurement errors.

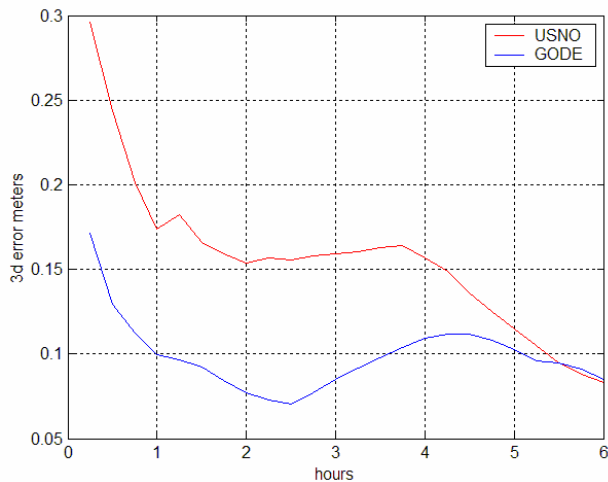


Figure 3. USNO and GODE 3-D position error

To confirm the results obtained at the USNO, we also used data from the nearby Goddard Space Flight Center (GODE) site. This site also features a hydrogen maser reference but does not have a met sensor. Therefore, the same met data from the USNO were used and data were processed over the same time interval. The results are shown in Figure 3 where a similar pattern is seen.

The above results are very comparable to those found in Witchayangcoon [2000], who also included CORS data from the USNO site, both in accuracy after six hours (10 cm) and rate of convergence. Witchayangcoon used a Kalman filter solution that incorporated both the pseudorange and carrier phase data. He also did not model phase windup. Witchayangcoon also used the Jet Propulsion Laboratory (JPL) automated data analysis service, which also gave an accuracy of about 10 cm.

SRI Data

Tests were then performed on the SRI campus in an area with particular multipath susceptibility. Figure 4 shows a photograph of the area around the GPS antenna. The GPS antenna is on a tripod located near the traffic cones just below the shadow of the dish antenna. The dish antenna is 6 meters in diameter and is located 8 meters above ground level and 15 meters away from the GPS antenna. The area is surrounded by buildings, metal truck trailers, and trees.



Figure 4. Antenna site

To estimate multipath at the site, data were collected for 24 hours with a Novatel OEM4 and TEQC was then run (Estey and Meertens, 1999). It was found that code multipath at L1 was 4 times that of the USNO site at zenith and 3.5 times at 30 degrees. Large numbers of cycle slips were shown to occur below 30 degrees.

The site survey was done using the Online Positioning Service from the National Geodetic Survey. The results are expected to be accurate to about 3 cm.

To give some indication of the multipath at the site, Figure 5 shows the time versus stand-alone 3-D position error from a Novatel OEM4 using a Novatel 502 antenna. Large excursions in position are observed as well as short-term instabilities.

Data were then collected for 24 hours using an OEM4, the next 24 hours using a PPS Ashtech XII receiver, and finally the next 24 hours with an SPS Ashtech XII. At the time of data processing no IGS final orbit was available so the rapid was used. Due to the relatively low quality of the data, many cycle slips had to be detected and removed.

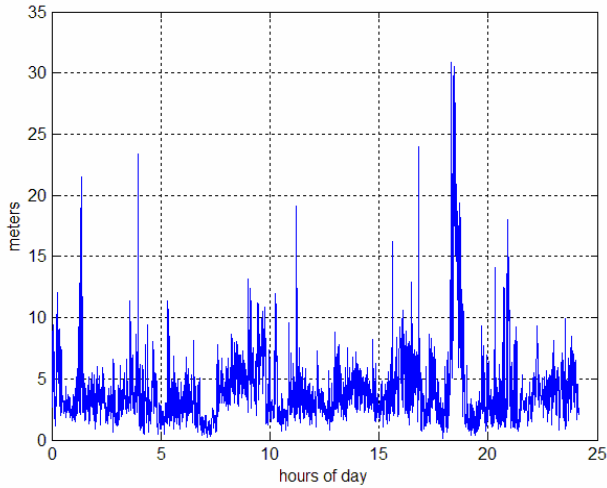


Figure 5. OEM 4 receiver 3-D error at SRI site

Figure 6 shows the 3-D position as a function of time for each of the three test cases. We also looked for component position biases in the results. Table 1 shows the results of the three receiver solution biases each in east, north, and vertical after six hours. The solutions show common biases, which is possibly due to the dish antenna. Further investigation needs to be done in this area.

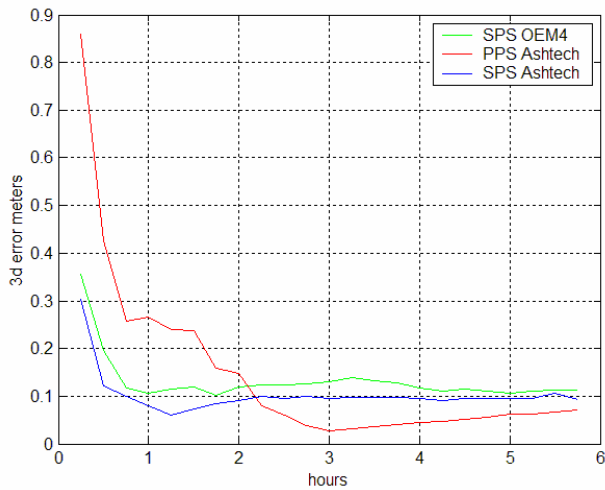


Figure 6. 3-D error for various configurations

Table 1. Component Position Errors for Various Configurations

	OEM4	Ashtech PPS	Ashtech SPS
East Bias (cm)	-6	-5	-6
North Bias (cm)	-6	-2	-5
Vertical Bias (cm)	6	4	4

The high multipath SRI data converged faster than the high quality USNO data. To show that this is probably due to the random nature of the data, the SPS Ashtech was processed using four different start times, each 15 minutes apart. As can be seen in Figure 7, this leads to large variations in the solution accuracy during the first hour, but similar values after that.

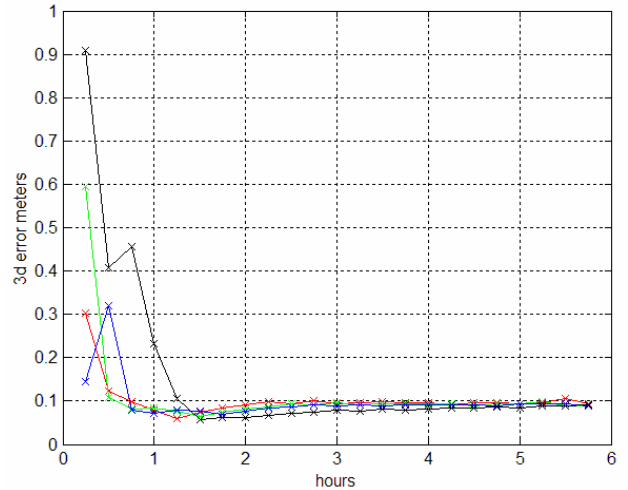


Figure 7. 3-D position error with different start times, SPS Ashtech

DISCUSSION/CONCLUSIONS

Four different methods of processing carrier phase data for PPP were considered and the position covariance for each method was evaluated. The TOA method was used for subsequent data analysis because its PDOP was the lowest in the short term than the other differencing methods. We have shown that after 15 minutes, an accuracy of well under a meter was attained. After an hour the accuracy generally improves to near a decimeter. The accuracy does not improve substantially after four hours, probably because of modeling errors.

A worthwhile experiment would be to try the other three methods to ensure that the above selection criteria are correct. While this has not been done, the rate of convergence and the final accuracy obtained were impressive. The accuracy could probably be further improved by taking into account predictable errors that were left out of the analysis, primarily phase windup, which can contribute up to a decimeter of error. Other factors contribute less error: ocean loading about a centimeter for the locations used (although much bigger for some island locations), atmospheric loading in the millimeters, and antenna phase center variations of about a centimeter (although this can have a larger effect if zenith tropospheric delay is treated as an unknown).

REFERENCES

- Abdel-Salam, M., Y. Gao, and X. Shen [2002] Analyzing the Performance Characteristics of a Precise Point Positioning System, Proceedings of the Institute of Navigation's ION GPS 2002, Portland, OR, pp. 1893–1899
- Bisnath, B.S., and R.B. Langley [2002] High-Precision, Kinematic Positioning with a Single GPS Receiver, *Navigation*, Vol. 49, No. 3.
- Estey, L.H. and M. Meertens [1999], TEQC: The Multi-Purpose Toolkit for GPS/GLONASS Data, *GPS Solutions*, Volume 3(1), Summer 1999.
- Kouba, J., [2002] A Guide to Using International GPS Service (IGS) Products, igs.cb.jpl.nasa.gov/components/IGSProducts_user_v17.pdf.
- Kouba, J., and P. Heroux [2000] GPS Precise Point Positioning Using IGS Orbit Products, www.geod.nrcan.gc.ca/index_e/products_e/publications_e/papers_e/final.pdf.
- Malys, S. and M.J. Ortiz [1989] Geodetic Absolute Positioning with Differenced GPS Carrier Beat Phase Data, Proceedings of the 5th International Geodetic Symposium on Satellite Positioning, Las Cruces, NM.
- Misra, P. and P. Enge [2001] Global Positioning System Signals, Measurements, and Performance, Ganga-Jamuna Press, Lincoln, MA.
- Niell, A.E. [1996] Global Mapping Functions for the Atmospheric Delay at Radio Wavelengths. *Journal of Geophysical Research*, **101**(B2):3227–3246.
- Shin, D., S. Son, and T. Sung [2000] DOP Relationship between the TOA and TDOA Positioning, Proceedings of the Institute of Navigation's Annual Meeting 2000, San Diego, CA, pp. 436–442.
- Skone, S., M.E. Cannon, K. Lochhead, P. Heroux, F. Lahaye [1996] Performance Evaluation of the NRCAN Wide Area System, Proceedings of the Institute of Navigation's ION GPS 1996, Kansas City, KA, pp. 1793–1802.
- Witchayangkoon, B. [2000] Elements of GPS Precise Point Positioning, Ph.D. Thesis, Univ. of Maine.
- Zumberge, J.F., M.B. Heflin, D.C. Jefferson, M.M. Watkins, and F.H. Webb [1997] Precise Point Positioning for the Efficient and Robust Analysis of GPS Data from Large Networks, *Journal of Geophysical Research*, Vol. 102, No. B3, pp. 5005–5017.